7

Fourier Transform Applications

7.1 SPECTRAL ANALYSIS

The raw complex-valued output of a fast Fourier transform (FFT) or discrete Fourier transform (DFT) is difficult to interpret directly. The most common approach is to present the ***power spectrum S*** of the given signal. Here the power for each frequency is plotted along the frequency axis (in Hz or in rad/s). This result is obtained by multiplying the FFT output X (Chapter 6, Equation (6.18)) with its complex conjugate X^*. Representing the DFT or FFT output for a given frequency ω_k as $a_k + jb_k$ (similar to Equation (6.15)), the power at ω_k is

$$(a_k + jb_k)(a_k + jb_k)^* = (a_k + jb_k)(a_k - jb_k) = a_k^2 + b_k^2$$

We used $j^2 = -1$, and the superscript * indicates the complex conjugate. Repeating this for all frequencies ω_k, the function defined over the whole spectrum S is

$$S = \frac{XX^*}{N} \tag{7.1}$$

The power spectrum can be normalized by dividing by the number of data points N. This normalization will ensure that the energy (sum of squares) of the time series equals the sum of the elements in the power spectrum (Appendix 7.1).

An example of applying spectral analysis to a short (8-point) time series is summarized in Table 7.1. The input time series is x consisting of eight ($n = 0 - 7$) real values; the output of the FFT is X, an array of eight complex values. It can be seen that the sum of squares in the time domain (column xx in Table 7.1) and the sum of the normalized power spectrum (S in Table 7.1) both equate to 107. The first value of the power spectrum quantifies the offset (DC component) which is the sum of the squares of all the values normalized by the number of values (Table 7.1)

$$\frac{\left(\sum_{i=0}^{7} x_i\right)^2}{N} = \frac{(-1)^2}{8} 0.125$$

Table 7.1 Example of an 8-point fft

Array x is the input and X the output of the algorithm. The real and imaginary parts are indicated in the fourth and fifth columns. The non-normalized power spectrum in the sixth column shows symmetry around $n = 4$ (not including the first value $n = 0$ representing the DC component). The real part of X is symmetric as well (corresponding to the even property of the cosine wave), whereas the imaginary part of X gains symmetry from the odd property of the sine wave. The sum of squares in the time domain (third column) and the normalized spectrum S (seventh column) is 107 in both cases. All values in the table were obtained using the MATLAB *fft* command.

n	x	xx	$R = real(X)$	$I = imag(X)$	XX^*	S	AS	ϕ
0	**0**	0	**−1**	**0**	1	0.125	0.25	0
1	**2**	4	**3.4853**	**−10.2426**	117.0589	14.6324	2.7048	−1.2428
2	**4**	16	**3**	**2**	13	1.625	0.9014	0.588
3	**−3**	9	**−13.4853**	**1.7574**	184.9411	23.1176	3.3998	−0.1296
4	**5**	25	**15**	**0**	225	28.125	3.75	0
5	**−7**	49	**−13.4853**	**−1.7574**	184.9411	23.1176	3.3998	0.1296
6	**−2**	4	**3**	**−2**	13	1.625	0.9014	−0.588
7	**0**	0	**3.4853**	**10.2426**	117.0589	14.6324	2.7048	1.2428
Sum	−1	107				107		

Further note that the power spectrum is symmetric around the midpoint ($n = 4$ in Table 7.1). Because of this symmetry, it is common practice to show only the values corresponding to positive frequencies. Therefore, to preserve the relationship between power in the time and frequency domains, some authors may normalize this one-sided spectrum by $2/N$.

A related approach to displaying the results of spectral analysis is to show the ***amplitude spectrum (AS)*** (Table 7.1), the square root of the power spectrum. If one wants the amplitude in the spectrum to correspond with the amplitude of sinusoidal signals in the time domain, one must normalize by $2/N$:

$$AS = \frac{2}{N}\sqrt{XX^*} \tag{7.2}$$

A third commonly used presentation is the ***phase spectrum***. This depicts the phase versus frequency, where phase ϕ is calculated as

$$\phi = \arctan\frac{I(X)}{R(X)} \tag{7.3}$$

with $I(X)$ and $R(X)$ denoting the imaginary and real parts of X, respectively. Unlike in the power and amplitude spectra, no normalization is required for the phase.

The ***X-axis of the spectrum*** is frequency. As mentioned earlier, since the full spectrum contains redundant information (Table 7.1), typically

only up to half of the spectrum is shown. Given a real-valued time series, we can establish that the power and amplitude spectra will be even functions; therefore, one half of the function represents all information. For example, if a time series is sampled at 1000 Hz and the FFT is calculated over 512 (2^9) points of the time series, the frequency axis range covering half the spectrum is

$$0 \rightarrow 1000 \times (512/2 - 1)/512\,\text{Hz} \approx (\text{sample rate})/2 \tag{7.4}$$

The 1 is subtracted from 512/2 because the frequency axis must begin at 0 (representing the DC component in the time domain). The step size on the frequency axis is $1000 \times 1/512$ Hz. For a spectral plot against angular frequency, the values in Hz must be by multiplied by 2π, and the step size becomes $1000 \times 2\pi \times 1/512$ rad/s.

This may seem overly technical, but the scaling makes perfect sense if we consider the following simple example. The signal's sample rate determines the highest frequency (Nyquist frequency, Chapter 2) that can be represented in the frequency domain. The epoch length determines the precision (e.g., a 500-point epoch sampled at 1000 Hz represents 0.5 s → the spectral resolution is the inverse of 0.5 s → 2 Hz). If we take a 1000-point epoch sampled at 200 Hz, the entire epoch is 5 seconds long, and the spectral resolution thus becomes 0.2 Hz (Fig. 7.1).

The signals in Figure 7.2 illustrate the use of spectral analysis to detect periodic elements within a noisy signal. The time domain signal contains noise plus both 50- and 120-Hz sine waves. ***You can use the following MATLAB script to recreate this example of spectral analysis.***

```
% pr7_1.m
% Spectrum

srate=1000;                          % sample rate
pt=512;                              % points (2n) for the FFT
range=(pt/2);                        % range for the spectral plot

t=0:1/srate:0.6;                     % time axis
f=srate*(0:range-1)/pt;              % frequency axis
                                     % starts at 0!
x=sin(2*pi*50*t)+sin(2*pi*120*t);    % SIGNALS 50 and 120 Hz
y=x+randn(1,length(t));              % signal + noise in mV

figure                               % plot signal
plot(t,y)
title('Time Series')
xlabel('time (s)')
ylabel('Amplitude (mV)')
```

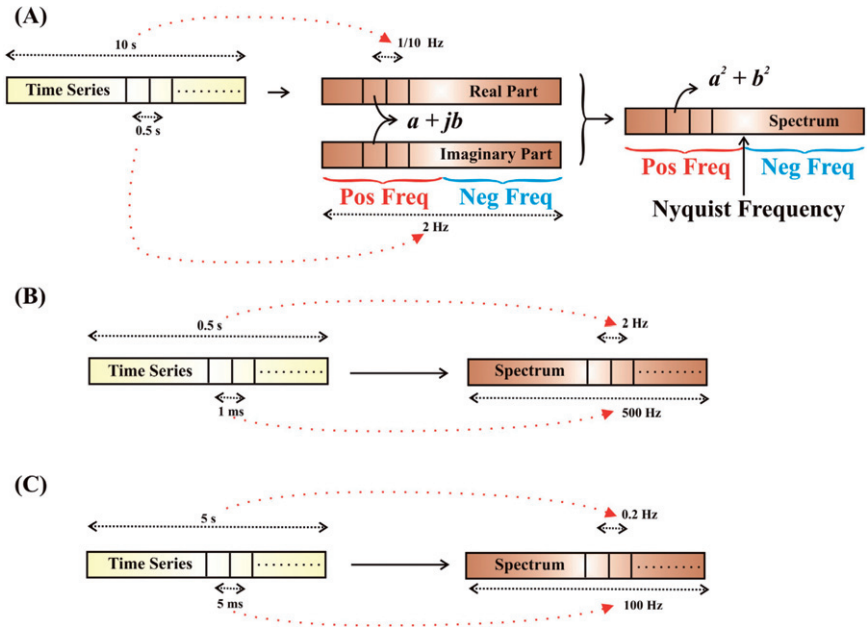

Figure 7.1 Overview of the relationships between the epoch length and sample rate of a time series with its precision and range in the associated spectrum. (A) An example of a time series sampled at an interval of one-half second for 10 seconds. The discrete Fourier transform consists of even (real) and odd (imaginary) parts in which the range (2 Hz) and resolution (1/10 Hz) are directly related to the time series. The spectrum resulting from these real and imaginary coefficients is even. The frequency scale can be represented as a full circle where $0 \rightarrow \pi$ can be considered as the positive frequencies and $\pi \rightarrow 2\pi$ as the negative ones. Because the power spectrum is even, the part reflecting the negative frequencies is identical to the part containing positive frequencies, and therefore it is common practice to depict only the first half of the spectrum (up to the Nyquist frequency). Two more examples with different sample rates and durations are shown in (B) and (C). (B) An example of a 0.5-s epoch sampled at 1 kHz (1-ms sample interval) resulting in 1/0.5 = 2-Hz precision and 1000/2 = 500-Hz range. (C) An example of a 5 s epoch sampled at 200 Hz (5-ms sample interval) resulting in 1/5 = 0.2-Hz precision and 200/2 = 100-Hz range. Note that in (B) and (C) only the positive frequencies are included in the spectrum.

```
Y=fft(y,pt);                          % do a 512 pt FFT
Pyy=Y.*conj(Y)/pt;                    % Power spectrum

figure                                % Plot result
plot(f,Pyy(1:range));                 % Pyy starts at 1 and f(1)=0
title('Powerspectrum')
xlabel('Frequency (Hz)')
ylabel('Power (mV2)')
```

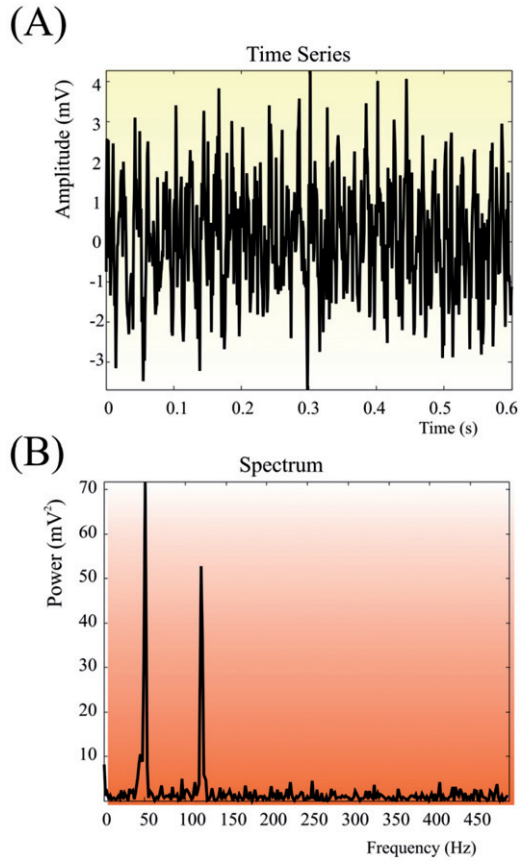

Figure 7.2 Output of the pr7_1.m script. (A) Time series. (B) Power spectrum. Note how the two sinusoidal signals at 50 and 120 Hz that are buried in noise (A) become clearly visible in the frequency domain (B).

A typical output of this script is shown in Figure 7.2. Please note that your output may be slightly different from the graphs in Figure 7.2 due to the random number generator randn used to simulate the noise component.

Spectral analysis is often used in EEG analysis to evaluate the classical EEG frequency bands (δ, θ, α, β; see Section 1.4.1). For this type of signal, the frequency domain characteristics are relevant because of the clinical significance of the various rhythms (Chapter 1, Fig. 1.2). The EEG and its associated spectrum in Figure 7.3 show a clear presence of the alpha rhythm, one of the most obvious components in the EEG in awake subjects with both eyes closed. The MATLAB file "AlphaRhythm_5seconds.mat," containing 5 s of the time domain signal recorded from

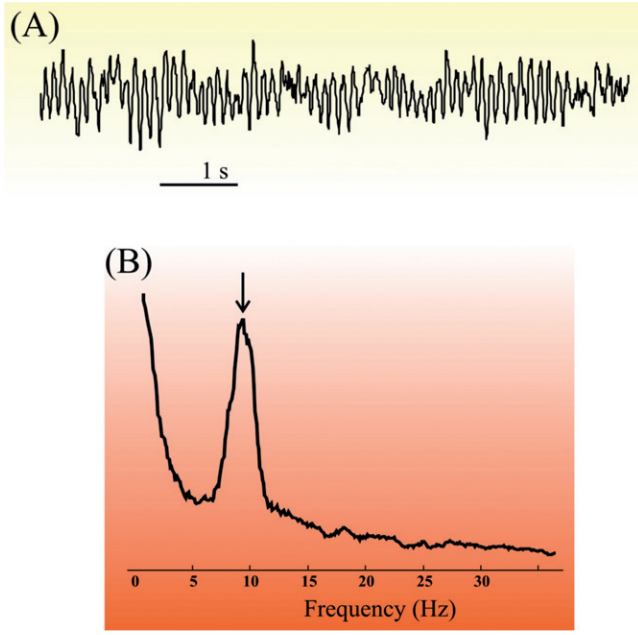

Figure 7.3 An example of spectral analysis of an EEG trace recorded from position O2 shown in (A). The trace includes strong oscillation in the alpha band. Accordingly, the power spectrum in (B) shows the clear presence of a component slightly below 10 Hz (arrow) representing this alpha rhythm. For clarity, the spectrum in (B) was smoothed using a rectangular 1.5-Hz window.

electrode position O2 and sampled at a rate of 250 Hz, is included on the CD.

7.1.1 Application of Data Windows

In the preceding examples, we determined the spectrum from a finite epoch of data. Because we evaluate the signal over a limited time interval consisting of N samples, we are implicitly multiplying the theoretically infinite input signal of the FFT (or DFT) algorithm with a rectangular function (i.e., a rectangular data window). As we will see in Chapter 8, this multiplication in the time domain corresponds with a convolution in the frequency domain. Because the DFT/FFT is determined by default over a limited epoch of a time series, we can analyze the effect of such a limitation using the continuous time Fourier transform (CFT). In the following example, we consider the transform of a cosine wave truncated by a finite epoch length. The theoretical transform for the continuous wave (Fig. 6.2C, Section 6.2.1) is composed of impulse functions at $\pm\omega_0$ — that is, the CFT pair is

$$\cos(\omega_0 t) \Leftrightarrow \pi[\delta(\omega + \omega_0) + \delta(\omega - \omega_0)] \tag{7.5}$$

Using Equation (6.4), we then obtain the Fourier transform $W_R(j\omega)$ of a rectangular window $w_R(t)$ function used to define our sampling epoch in time. The rectangular window is equal to one only for the duration of the epoch from $-T/2$ to $T/2$, and zero everywhere else. We use the fact that $w_R(t) = 0$ for $|t| > T/2$ to change the integration limits in the Fourier transform integral; therefore, the CFT for the window we use as the input for the DFT analysis is

$$\begin{aligned} W_R(j\omega) &= \int_{-\infty}^{\infty} w(t) e^{-j\omega t} dt = \int_{-T/2}^{T/2} 1 e^{-j\omega t} dt = -\frac{1}{j\omega}\left[e^{-j\omega t}\right]_{-T/2}^{T/2} \\ &= -\frac{1}{j\omega}\left[e^{-j\omega T/2} - e^{j\omega T/2}\right] = -\frac{1}{j\omega}[-2j\sin(\omega T/2)] \\ &= \frac{2\sin(\omega T/2)}{\omega} = \frac{\sin(\pi f T)}{\pi f} \end{aligned} \tag{7.6}$$

In the last steps in Equation (7.6), we used Euler's relationship [$e^{jx} = cos(x) + j\ \sin(x)$], and $2\pi f$ was substituted for ω.

We can plot the power of this function against frequency for different widths of the window (Fig. 7.4). With increasing width (T), we observe that (1) the amplitude of the main peak and its associated ripples increases, and (2) the width of these features decreases. The example in Figure 7.4 shows that the spectrum of the window has a ripple at the frequency equal to the inverse of the duration of the window. When analyzing a pure wave at frequency f, this ripple effect results in the "leaking" of energy around the spectral peak f.

The leaking of energy to adjacent frequency bands is due to the fact that the multiplication of the time domain wave with a rectangular window is equivalent to a complex convolution in the frequency domain (Chapter 8). If you are not yet familiar with convolution, you may skip this paragraph and come back to it later. Combining Equations (7.5) and (7.6), we can evaluate the effect of a rectangular window in the time domain on the spectral analysis of a pure cosine wave. We may use complex convolution to describe the Fourier transform pair

$$w_R(t) \times \cos(\omega_0 t) \Leftrightarrow \frac{1}{2\pi}\int_{-\infty}^{\infty} [W_R(j\omega - ju)]\pi[\delta(u + \omega_0) + \delta(u - \omega_0)]du \tag{7.7}$$

Using the sifting property of the Dirac delta function to evaluate the integral,

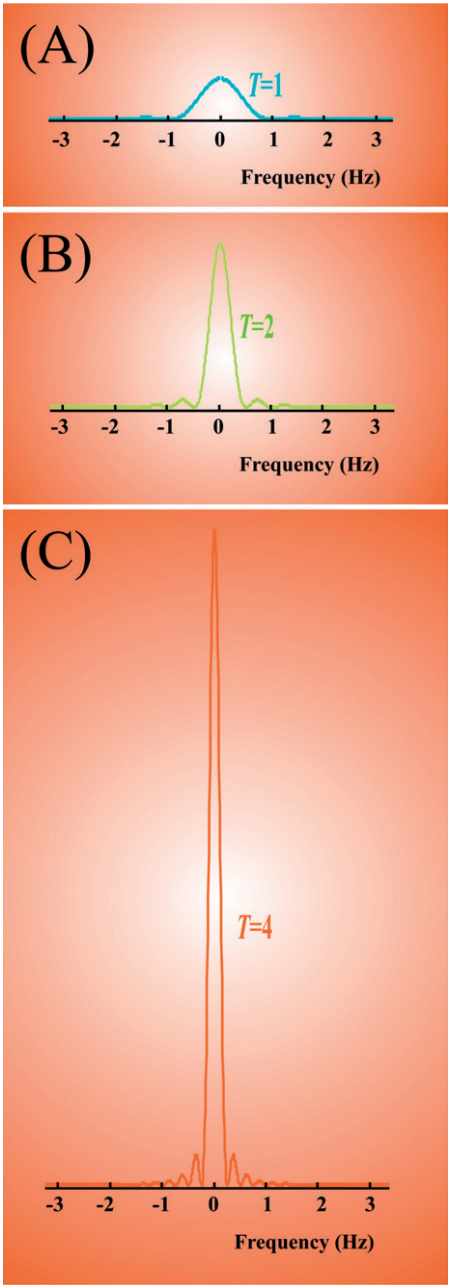

Figure 7.4 The ***power spectrum*** of rectangular windows of duration $T = 1$, 2, and 4. It can be seen that these spectra have ripples in the frequency domain that correspond to the inverse of their window duration (i.e., for $T = 4$ the ripples are at $\frac{1}{4}$ Hz, for $T = 2$ the ripples are at $\frac{1}{2}$ Hz, and for $T = 1$ the ripples are at 1 Hz). This ripple effect causes the discrete spectrum of a pure wave such as $\cos(2\pi ft)$ or $\sin(2\pi ft)$ to show energy adjacent to the main peak at frequency f. The vertical calibration is in arbitrary units but is identical for all panels.

$$w_R(t) \times \cos(\omega_0 t) \Leftrightarrow \int_{-\infty}^{\infty} \left[\frac{\sin(\omega - u)T/2}{\omega - u}\right][\delta(u + \omega_0) + \delta(u - \omega_0)]du$$
$$= \frac{\sin((\omega + \omega_0)T/2)}{\omega + \omega_0} + \frac{\sin((\omega - \omega_0)T/2)}{\omega - \omega_0} \quad (7.8)$$

Interpreting Equation (7.8), we conclude that the spectrum of a truncated cosine wave with a frequency ω_0 produces a broadened peak surrounded by ripples (identical to the function in Figure 7.4) at $\pm\omega_0$ in the frequency domain. This process of multiplication in the time domain and convolution in the frequency domain for the truncated cosine is summarized in Figure 7.5.

More deliberately crafted time domain windowing functions (to replace the implicit rectangular window) are commonly applied to avoid the ugly ripple effects in the spectra. This reduction in ripples comes at a cost. For each sine/cosine wave, the window attenuates the amplitude of the spectral peak and increases its width. Several commonly applied data windows are summarized in Table 7.2. In MATLAB, these windows are included in the Signal Processing Toolbox. Examples of the bartlett, boxcar (rectangular), and hanning windows are depicted in Figure 7.6.

Note: A window that transforms into a flat line in the frequency domain seems to be the simple solution to avoiding all the undesired effects we discussed earlier. This would result in a complex convolution result that does not distort the spectrum of the signal at hand. Unfortunately, such a flat line in the frequency domain does not transform well into a finite window in the time domain.

Table 7.2 Overview of Commonly Used Data Window Functions

Data window	Equation window $w(t)$ for epoch size $-T \rightarrow T$
Bartlett (Triangular, Fejér)	$w(t) = \begin{cases} 1 - \frac{\lvert t\rvert}{T} & \lvert t\rvert \le T \\ else\ 0 \end{cases}$
Hamming	$w(t) = \begin{cases} 0.54 + 0.46\cos\left[\frac{\pi t}{T}\right] & \lvert t\rvert \le T \\ else\ 0 \end{cases}$
Hann (von Hann, Hanning)	$w(t) = \begin{cases} 0.5 + 0.5\cos\left[\frac{\pi t}{T}\right] & \lvert t\rvert \le T \\ else\ 0 \end{cases}$
Rectangular	$w(t) = \begin{cases} 1 & \lvert t\rvert \le T \\ else\ 0 \end{cases}$

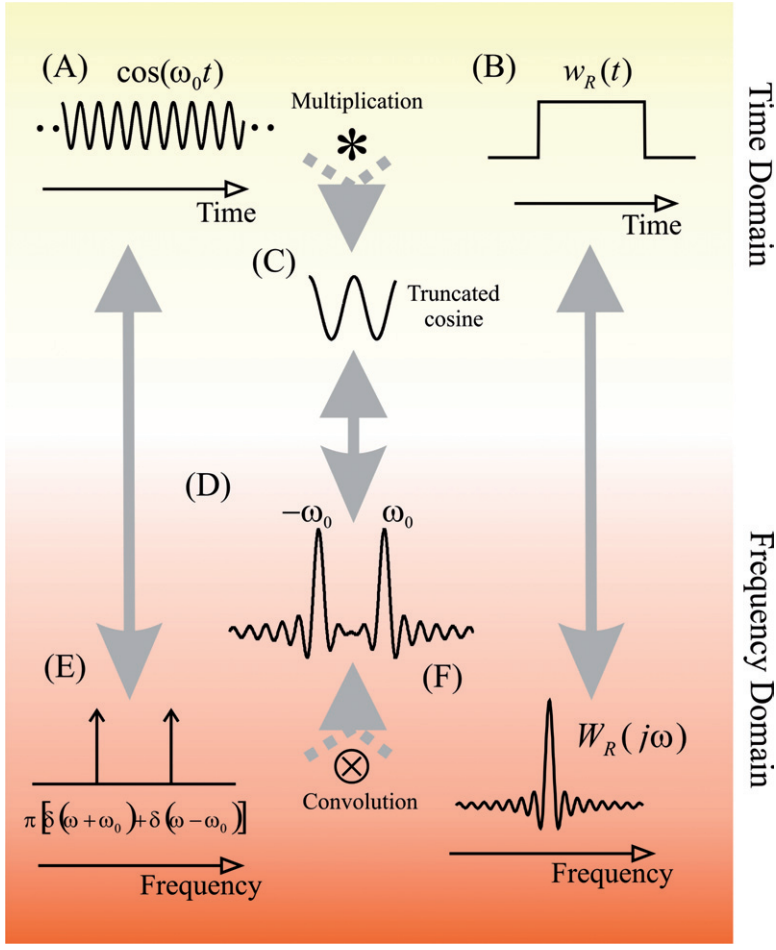

Figure 7.5 Overview of the Fourier transform of a truncated cosine wave. A theoretically infinite cosine wave (A) multiplied by a rectangular window (B) generates a truncated wave (C). The Fourier transform of the cosine and the window in the frequency domain are shown in (E) and (F), respectively. The transform of the truncated cosine is the convolution of its components, shown in (D).

7.1.2 Spectral Analysis of Physiological Signals

Spectral analysis of signals composed of pure sine waves is theoretically straightforward. In physiological signals, interpretation of spectra requires caution because these time series are rarely stationary and usually contain both nonperiodic and periodic components. Even when the DC component is removed, the spectra from physiological data may contain low-

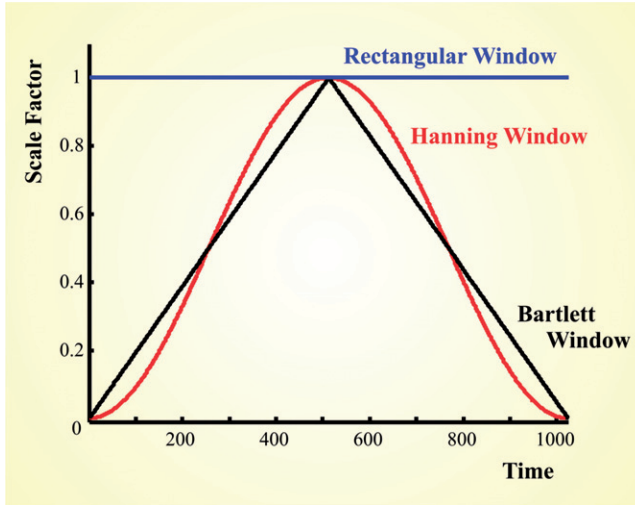

Figure 7.6 Examples of three window functions of 1024 points.

frequency components due to slow nonperiodic activity (e.g., trends) or periodic activity with a periodicity beyond the analysis window. Similarly, the high-frequency components may be contaminated by high-frequency nonperiodic processes (e.g., sudden events). Furthermore, the periodic activity in physiological signals is usually far from purely sinusoidal, leading to spectral components (so-called harmonics) at higher frequencies.

The take-home message from this discussion is that not all peaks in a spectrum of physiological data directly correspond to actual physiological, periodic processes in the system at hand. Careful evaluation must be used to distinguish between real spectral peaks and irrelevant by-products. A somewhat trivial example showing the effect of a not exactly sinusoidal signal is the respiratory signal depicted in Figure 7.7. Although the actual respiratory rhythm cycles at around 1.5 Hz, the spectrum shows a harmonic at ~3 Hz.

7.2 TOMOGRAPHY

Thus far we have applied the Fourier transform to one-dimensional time series. Here we apply the transform to a problem in tomography used in medical imaging. In this section, we approach tomography in a general fashion; the principles we discuss apply both to scanning emission and absorption profiles. Consider emission of activity and passive absorption

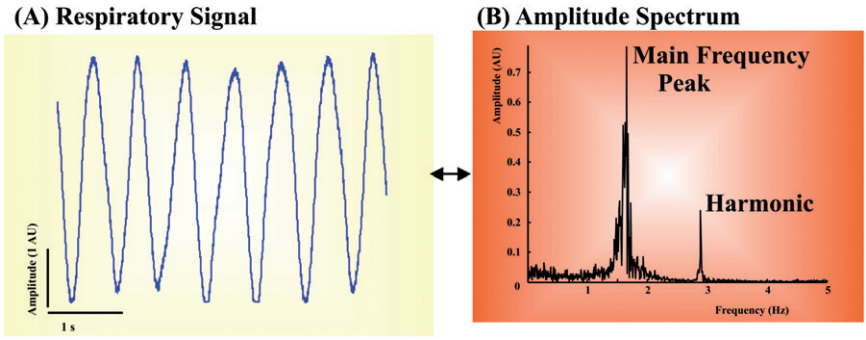

Figure 7.7 Frequency analysis of a respiratory signal from a human neonate. An epoch of the time domain signal is shown in (A) and the amplitude spectrum in (B). Clearly the main peak ~1.5 Hz shows the respiratory frequency, whereas the peak close to 3 Hz is a harmonic due to the imperfect sinusoidal signal. The respiration signal, sampled at 1 kHz, is available on the CD (respiration.mat).

as the same type of process. In the case of emission, each little voxel (or pixel in the two-dimensional case) emits its own contribution to the total that is measured outside the volume. The absorption model is slightly more complicated since each pixel instead contributes to attenuation across the area. We can use Beer's law to express the intensity of the output I_o of a beam as a function of input intensity I_i and attenuation caused by absorption a_k in N elements: $I_o = I_i e^{-\sum_{k=1}^{N} a_k}$. Using the property that the absorption law is exponential, we can use the logarithm of the absorption ratio A to obtain an additive effect for each element k — that is,

$$A = \ln\left[\frac{I_o}{I_i}\right] = \sum_{k=1}^{N} a_k \tag{7.9}$$

7.2.1 Measured Absorption — Radon Transform

In the following discussion, we develop the ***Radon transform***, the ***Fourier slice theorem***, and ***filtered back projection*** as each applies to MRI and CT image reconstruction. These techniques require reconstruction of a density function representing the internal structure of an object from sensor readings taken from outside that object. This is typically accomplished by calculating a series of two-dimensional density functions (or slices) through the object on a set of planes and reconstructing the three-dimensional image from those images. Thus, the fundamental problem in both of these techniques is the calculation of the two-dimensional density function with readings from a sensor, which typically rotates around the

object on the given plane. The following derivations use Fourier analysis to relate a filtered version of this measured signal to the density function of an object within the measured region.

Our goal is to scan an object enclosed in a circle with radius R. For ease of explanation, we use polar coordinates to derive the theorem. Assume a source and detector moving along a line at an angle θ with respect to the x-axis Fig. 7.8. The distance of the source-detector (SD) line from the origin is t, and the detector measures absorption (or emission) of all the points along the line. In polar coordinates, all points r,ϕ on the SD line, relate to t as

$$t = r\cos(\phi - \theta) \tag{7.10}$$

If the emitter/detector pair moves at a constant speed, t represents time and the measurement at the detector becomes a time series. The Radon transform describes the measured values for t and θ.

The value of θ varies between 0 and 180 degrees. The total absorption along SD is represented by $m(t, \theta)$ and is determined by the contributions of arbitrarily small surfaces $r\ dr\ d\phi$ (see inset in Fig. 7.8). Denoting the absorption function inside the circle as $a(r, \phi)$, which corresponds to the mass to be scanned, we obtain

$$m(t,\theta) = \int\int_R a(r, \phi)\delta[t - r\cos(\phi - \theta)]rdrd\phi \tag{7.11}$$

Think of $\int\int_R a(r, \phi)$ as the total absorption of the whole object inside the circle with radius R. For a particular measurement $m(t, \theta)$, we are only interested in the contributions along the line of response (LOR, Fig. 7.8). We pull these out by adding a δ function that sifts for the values for ϕ and r on the LOR at a given t and θ. The delta function that accomplishes this must evaluate to zero within the LOR — that is, the argument should be $t - r\cos(\phi - \theta) = 0$, and $\delta[t - r\cos(\phi - \theta)]$ in Equation (7.11) accomplishes sifting the points on the LOR. Using integration limits reflecting area R instead of $-\infty \to \infty$ is appropriate because $a(r, \phi) = 0$ for $r > R$.

The one-dimensional continuous Fourier transform of $m(t, \theta)$ in the spatial domain is

$$M(z,\theta) = \int_{-\infty}^{\infty} m(t, \theta)e^{-j2\pi zt}dt \tag{7.12}$$

where z represents the spatial frequency domain. Substituting (7.11) in (7.12) and combining all terms related to t within the square brackets gives

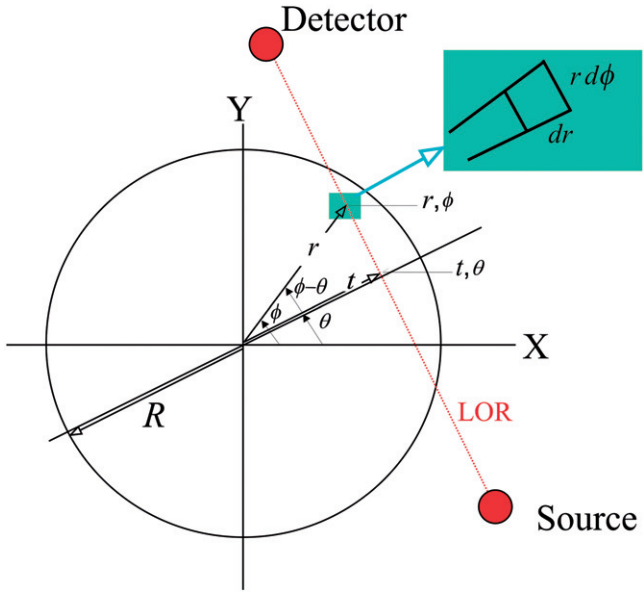

Figure 7.8 Diagram of a CT scan procedure with a source-detector setup scanning an object within a circle with radius R.

$$M(z,\theta)=\iint_R a(r,\phi)\left[\int_{-\infty}^{\infty}\delta[t-r\cos(\phi-\theta)]e^{-j2\pi zt}dt\right]rdrd\phi \tag{7.13}$$

Using the sifting property of the δ function for the integration over t, Equation (7.13) becomes

$$\boxed{M(z,\theta)=\iint_R a(r,\phi)e^{-j2\pi zr\cos(\phi-\theta)}rdrd\phi} \tag{7.14}$$

In the following section, we will show that this expression is identical to the two-dimensional Fourier transform of the absorption function a.

7.2.2 The Absorption Function in the Spatial Frequency Domain

The two-dimensional Fourier transform of the absorption function $a(x, y)$ in Cartesian coordinates is

$$A(u,v)=\int_{-\infty}^{\infty}\int_{-\infty}^{\infty}a(x,y)e^{-j2\pi(xu+yv)}dxdy \tag{7.15}$$

Changing u and v into polar coordinates z and θ gives

$$A(z\cos\theta, z\sin\theta) = \int_{-\infty}^{\infty}\int_{-\infty}^{\infty} a(x,y)e^{-j2\pi z(x\cos\theta + y\sin\theta)}dxdy \tag{7.16}$$

Similarly, transforming x and y to polar coordinates r and ϕ gives

$$A(z,\theta) = \int_{-\infty}^{\infty}\int_{-\infty}^{\infty} a(r\cos\phi, r\sin\phi)e^{-j2\pi zr(\cos\phi\cos\theta + \sin\phi\sin\theta)}rdrd\phi \tag{7.17}$$

Using the trigonometric identity $\cos\phi\cos\theta + \sin\phi\sin\theta = \cos(\phi - \theta)$ and setting $a(r, \phi) = 0$ for all points outside the circle with radius R, Equation (7.17) becomes

$$\boxed{A(z,\theta) = \int_R\int a(r,\phi)e^{-j2\pi zr\cos(\phi-\theta)}rdrd\phi} \tag{7.18}$$

7.2.3 The Fourier Slice Theorem

The two-dimensional Fourier transform of the absorption function a evaluates to the same expression as the one-dimensional transform of the measured Radon transform m (Equations (7.14) and (7.18)) — that is,

$$\boxed{A(z,\theta) = M(z,\theta)} \tag{7.19}$$

Equation (7.19) is known as the ***Fourier slice theorem***.

7.2.4 The Inverse Transform

The inverse transform of Equation (7.18) returns $A(z, \theta)$ to the spatial domain

$$a(r,\phi) = \int_{-\infty}^{\infty}\int_{-\infty}^{\infty} A(z,\theta)e^{j2\pi zr\cos(\phi-\theta)}zdzd\theta \tag{7.20}$$

Using Equation (7.19) and defining $G(z, \theta) = z\,M(z, \theta)$, Equation (7.20) becomes

$$a(r,\phi) = \int_{-\infty}^{\infty}\int_{-\infty}^{\infty} G(z,\theta)e^{j2\pi zr\cos(\phi-\theta)}dzd\theta \tag{7.21}$$

The seemingly arbitrary multiplication of $M(z, \theta)$ with z in the frequency domain equates to convolution of $m(t, \theta)$ with a high-pass filter characteristic in the spatial domain (Chapter 12). The inverse transform of

$G(z, \theta)$ is $g(t, \theta)$ and can therefore be considered a high-pass filtered (differentiated) version of $m(t, \theta)$.

If we focus on the integration to dz in the preceding expression, the part $\int_{-\infty}^{\infty} G(z,\theta)e^{j2\pi zr\cos(\phi-\theta)}dz$ can be written as

$$\int_{-\infty}^{\infty} G(z,\theta)e^{j2\pi zw}dz \quad \text{with} \quad w = r\cos(\phi-\theta) \tag{7.22}$$

Recognizing this as the inverse Fourier transform of $g(w, \theta)$ and changing the integration limits for θ to $0 \rightarrow 180$ degrees (or $0 \rightarrow \pi$ radian), Equation (7.21) evaluates to

$$a(r,\phi) = \int_0^{\pi} g(w,\theta)d\theta = \int_0^{\pi} g(r\cos(\phi-\theta),\theta)d\theta \tag{7.23}$$

Because the function $g(\ )$ is a filtered/differentiated version of $m(\ )$, Equation (7.23) is the ***filtered backprojection equation***.

7.2.5 Backprojection in Cartesian Coordinates

For ease of use, we can transform Equation (7.23) from polar to Cartesian coordinates. We use

$$\cos\phi\cos\theta + \sin\phi\sin\theta = \cos(\phi-\theta)$$

Now Equation (7.23) can be written as

$$a(r,\phi) = \int_0^{\pi} g[r\cos(\phi)\cos(\theta) + r\sin(\phi)\sin(\theta), \theta]d\theta \tag{7.24}$$

With

$$r = \sqrt{x^2+y^2} \quad x = r\cos(\phi) \quad y = r\sin(\phi)$$

Equation (7.24) becomes

$$a(x,y) = \int_0^{\pi} g[x\cos\theta + y\sin\theta, \theta]d\theta \tag{7.25}$$

For a given θ, the original measurement of $m(\ )$ and its filtered version $g(\ )$ (for a given θ) are ordered according to the variable t; we use the following to relate t to x, y, and θ: $t = x\cos\theta + y\sin\theta$ (i.e., the standard procedure to recalculate the new x-coordinate after a counterclockwise axis rotation of θ degrees).

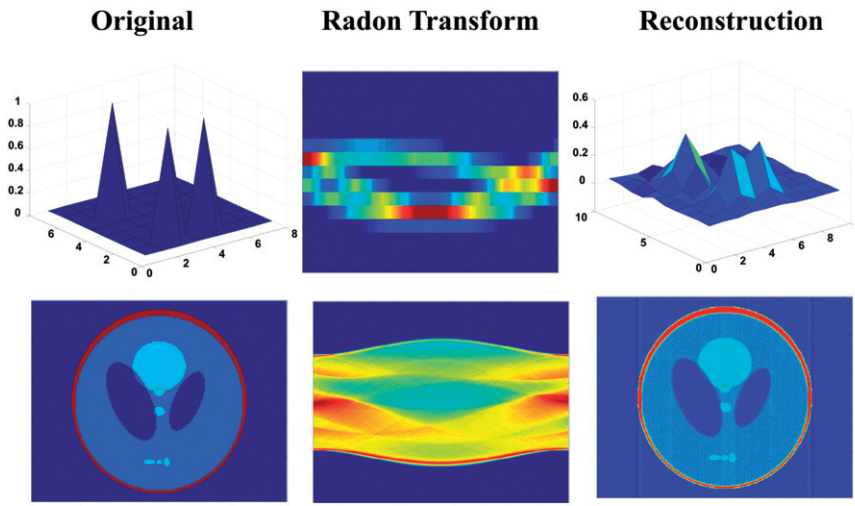

Figure 7.9 Examples of reconstruction of an image. The upper row represents the transform and reconstruction of an image (shown as a surface) composed of three pixels set to one in a field of zeros. The lower row is a similar example using the modified Shepp-Logan phantom available in MATLAB's image processing toolkit.

***The image processing toolbox in MATLAB contains commands for the Radon transform and its inverse. The script pr7_2 uses these commands for the Shepp-Logan phantom* (*Fig. 7.9*).**

```
% pr7_2
clear

P=phantom('Modified Shepp-Logan');

figure                          % Depict P
imagesc(P)

% Create Projections
theta=0:1:180;                  % steps of theta
R=radon(P,theta);               % radon transform
figure; imagesc(R);             % show radon transform

figure;
for step=1:20;
   theta=0:step:180;
   Rtemp=R(:,theta+1);
```

```
    p=iradon(Rtemp,theta);      % perform filtered backprojection
                                % NOTE: the iradon transform
                                % includes high pass filtering

    imagesc(p);                 % show result at each resolution 'step'
    drawnow
    pause                       % pause before proceeding to the next
end;
```

APPENDIX 7.1

Parseval's theorem states that the energy of a signal in the time domain equals the energy of the transformed signal in the frequency domain. Preservation of this equality is the underlying reason why the spectrum is normalized by 1/N in Equation (7.1). To understand this normalization, we will first determine what the relationship is between the energy of a time series and its equivalent representation as a complex Fourier series. From this result, we will subsequently develop the normalization for the DFT (Fig. A7.1).

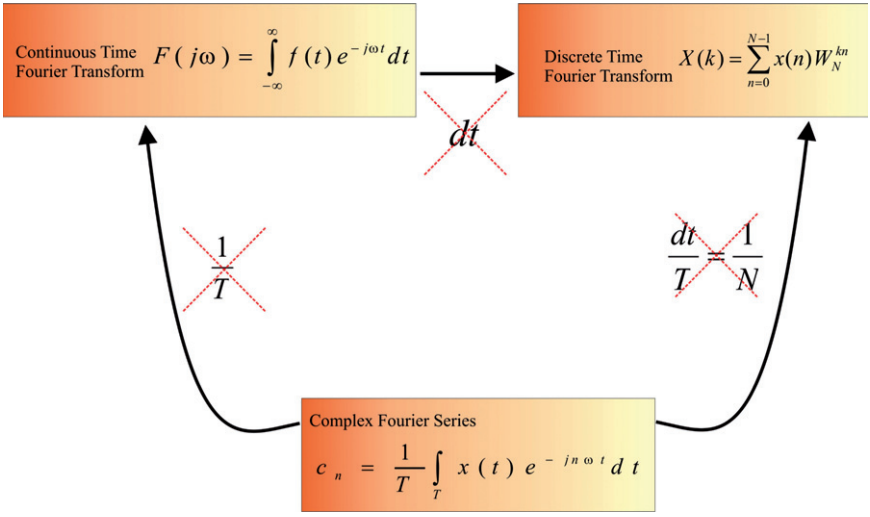

Figure A7.1 Overview of normalizations in the different flavors of the Fourier analysis. This diagram shows that the continuous Fourier transform relative to the Fourier series loses a factor $1/T$. The discrete Fourier transform loses a factor dt relative to the continuous time transform. Combining these two factors demonstrates that the DFT differs from the Fourier series by a factor $dt/T = 1/N$.

Consider three finite time series $f(t)$, $f_1(t)$, and $f_2(t)$ periodic over period $T = N\Delta t$, with $f(t) = f_1(t)\, f_2(t)$. For each of the time series, we can generate the complex Fourier series (Equations (5.19) and (5.20)):

$$\begin{aligned} f_1(t) &= \sum_{n=-\infty}^{\infty} d_n e^{jn\omega t} \leftrightarrow d_n = \frac{1}{T}\int_T f_1(t) e^{-jn\omega t} dt \\ f_2(t) &= \sum_{n=-\infty}^{\infty} g_n e^{jn\omega t} \leftrightarrow g_n = \frac{1}{T}\int_T f_2(t) e^{-jn\omega t} dt \\ f(t) &= \sum_{n=-\infty}^{\infty} c_n e^{jn\omega t} \leftrightarrow c_n = \frac{1}{T}\int_T f(t) e^{-jn\omega t} dt \end{aligned} \tag{A7.1-1}$$

Using the relationship between the three signals, we can write c_n as

$$c_n = \frac{1}{T}\int_T f_1(t) f_2(t) e^{-jn\omega t} dt \tag{A7.1-2}$$

Replacing f_1 by its Fourier series,

$$c_n = \frac{1}{T}\int_T \left(\sum_{m=-\infty}^{\infty} d_m e^{jm\omega t} \right) f_2(t) e^{-jn\omega t} dt \tag{A7.1-3}$$

and changing the order of the integral and summation operations results in

$$c_n = \sum_{m=-\infty}^{\infty} d_m \left(\frac{1}{T}\int_T f_2(t) e^{-j(n-m)\omega t} dt \right) \tag{A7.1-4}$$

Using Equation (A7.1-1), the terms in between the brackets can be set to g_{n-m}:

$$c_n = \frac{1}{T}\int_T f_1(t) f_2(t) e^{-jn\omega t} dt = \sum_{m=-\infty}^{\infty} d_m g_{n-m} \tag{A7.1-5}$$

For $n = 0$, we get

$$\frac{1}{T}\int_T f_1(t) f_2(t) dt = \sum_{m=-\infty}^{\infty} d_m g_{-m} \tag{A7.1-6}$$

To evaluate the power of a single time series x, we can substitute functions $x(t)$ and $x^*(t)$ for $f_1(t)$ and $f_2(t)$:

$$P = \frac{1}{T}\int_T x(t) x^*(t) dt \tag{A7.1-7}$$

The * in $x^*(t)$ indicates the complex conjugate of $x(t)$. The complex Fourier series and coefficients of $x(t)$ and $x^*(t)$ can be determined with

$$x(t) = \sum_{m=-\infty}^{\infty} h_n e^{jn\omega t} \leftrightarrow h_n = \frac{1}{T}\int_T x(t)e^{-jn\omega t}$$
$$x^*(t) = \sum_{m=-\infty}^{\infty} y_n e^{jn\omega t} \leftrightarrow y_n = \frac{1}{T}\int_T x^*(t)e^{-jn\omega t}dt \quad \text{(A7.1-8)}$$

The expression for y_n can be written as

$$y_n = \left(\frac{1}{T}\int_T x(t)e^{jn\omega t}dt\right)^* = h^*_{-n} \quad \text{(A7.1-9)}$$

Combining Equations (A7.1-9), (A7.1-6), and (A7.1-7),

$$\frac{1}{T}\int_T x(t)x^*(t)dt = \sum_{m=-\infty}^{\infty} h_n h_n^*$$
$$\rightarrow \frac{1}{T}\int_T |x(t)|^2 dt = \sum_{m=-\infty}^{\infty} |h_n|^2 \quad \text{(A7.1-10)}$$

Note that g_{-m} from Equation (A7.1-6) is substituted by $h^*_{-(-n)} = h_n^*$ in Equation (A7.1-10).

Finally we translate the relationship in Equation (A7.1-10) for the complex Fourier series into the DFT of a signal with finite duration. The expression remaining on the left-hand side in (A7.1-10) becomes $\frac{1}{N}\sum_{n=0}^{N-1} x^2(n)$. The expression to the right of the equal sign is proportional to the DFT but must be corrected by a factor $1/T_0$ (Section 6.2) and Δt (Section 6.3.1) (i.e., $\Delta t/T_0 = 1/N$) (see the diagram in Figure A7.1-1). Using $X(k)$ to denote the DFT and taking into account this correction, the expression on the right-hand side of Equation (A7.1–10) becomes $\sum_{k=0}^{N-1}\frac{1}{N}X(k)\frac{1}{N}X^*(k) \rightarrow \frac{1}{N^2}\sum_{k=0}^{N-1}|X(k)|^2$. Combining the preceding, we obtain Parseval's identity for the DFT:

$$\frac{1}{N}\sum_{n=0}^{N-1} x^2(n) = \frac{1}{N^2}\sum_{k=0}^{N-1}|X(k)|^2 \rightarrow \sum_{n=0}^{N-1} x^2(n) = \frac{1}{N}\sum_{k=0}^{N-1}|X(k)|^2 \quad \text{(A7.1-11)}$$

In Equation (A7.1-11), we see that the energy in the time series $x(n)$ can be related to the energy in the spectrum by the factor $1/N$. This is the underlying reason for the normalization of $X(k)$ $X^*(k)$ by $1/N$ in Equation (7.1). Of course, one might disagree with this approach and prefer the normalization that derives from the amplitude (i.e., normalize by $1/N^2$). Again if you only show half of the power spectrum, you must multiply the correction factor by 2, giving correction factors of $2/N$ or $2/N^2$.